Seismic vulnerability of structures - Application to the Civil Protection building in Andorra

M. BARUS[a], O. DALVERNY[b], H. WELEMANE[c], J.P. FAYE[d], C. MARTIN[e]

a. Laboratoire Génie de Production (LGP), INP-ENIT, Univ de Toulouse, Tarbes (matthias.barus@enit.fr)
b. Laboratoire Génie de Production (LGP), INP-ENIT, Univ de Toulouse, Tarbes (olivier.dalverny@enit.fr)
c. Laboratoire Génie de Production (LGP), INP-ENIT, Univ de Toulouse, Tarbes (helene.welemane@enit.fr)
d. Laboratoire Génie de Production (LGP), INP-ENIT, Univ de Toulouse, Tarbes (jp.faye@enit.fr)
e. Laboratoire Génie de Production (LGP), INP-ENIT, Univ de Toulouse, Tarbes (carmen.martin@enit.fr)

Abstract :

This works deals with the seismic vulnerability of buildings in the Pyrenees mountains region where almost a thousand earthquakes are recorded each year in the border area. The challenge is twofold : first to detect the damage due to seismic events and then to localize it inside studied buildings. Operational Modal Analysis (OMA) coupled with numerical modelling by Finite Element (FE) constitutes an interesting approach to address these issues. Here we intend to apply such methodology on a concrete building located in Andorre-la-Vieille (Edifici administratiu del Prat del Rull del govern d'Andorra). This building is a strategic place because it is where the Civil Protection Department of the Andorra Principality is based. The structural behaviour of the building is studied through frequency computation method in order to identify its undamaged behaviour. A seismic event is next simulated by a non-linear dynamic computation method which creates damage within the structure. Numerical results (eigen frequency, modal shapes and damage location) allow to highlight damaged zones induced by the earthquake and quantify degradation level in these areas. Accordingly, some guidelines may be given in view of the future instrumentation of the building (accelerometers and RAR).

Keywords : seismic damage, operational modal analysis, finite element modelling, frequency computation method

1 Introduction

This work is a part of the cross-border area POCRISC project. POCRISC EFA158/16 project is $65\,\%$ financed by the European Regional Development Fund (ERDF) through the Interreg V-A Spain France Andorra program (POCTEFA 2014-2020). POCTEFA aims to reinforce the economic and social integration of the French-Spanish-Andorran border. Its support is focused on developing economic, social and environmental cross-border activities through joint strategies favouring sustainable territorial development. The project started in January 2018 and lasts 3 years (2018-2020). The objective of this international collaboration (concerning regions of Catalonia in Spain, Occitania in France and Andorra) is to develop a common culture of the seismic risk in the Pyrenees in order to harmonize approximations of the seismic vulnerability and risk, and thereby promote the dissemination of the common and shared information to both local authorities and the public. At the same time, it is intended to provide tools to decision help adapted to necessities of seismic crisis managers.

Every year, a thousand earthquakes are recorded in Pyrenees, $90\,\%$ of them in a strip about $50\,\mathrm{km}$ around the border [1]. Since 2013, there have been, about fifteen M > 3 seismic events in the Pyrenees each year [2]. These work deals with assessing structure damaging and its impact on the population in the affected areas. Precisely, it addresses the two first Structural Health Monitoring (SHM) levels namely : damage detection and damage localization. Assessing buildings structural integrity can be achieved by several kinds of non-destructive techniques such as : visual inspection, stress-wave methods (acoustic emission, impact echo testing...), electro-magnetic methods (ground penetration radar, electrical resistivity measurements...), thermal methods (infrared thermography) or Vibration Based Damage Detection Methods (VBDDM, dynamic/vibration testing). However, one of them, the VBDDM are the most commonly used for measuring the structural integrity of structure [3]. Determining if a structure is damaged or not can be achieved experimentally using VBDDM in which Operational Modal Analysis (OMA) helps for studying the changes of its dynamical characteristics [4, 5]. Indeed, the damaging of a structure induces by an earthquake leads to the modification of its mechanical behaviour. In particular, a damaged structure shows a least rigidity than an undamaged structure and thus a higher damping. This results in a modification of the dynamic characteristics such as the reduction of eigen frequencies and modification of modal shapes [6, 7]. Studying these changes and determining the state of a structure at a given time can be achieved through the processing of experimental data captured by a few of sensors. Defining the accurate location of a damage is however quite less trivial. Several OMA methods allow localizing a structural damage with various success. As example, methods linked to modal shape variations (mode shape curvature and curvature damage factor methods) are sensitive to measurement directions while flexibility variations based methods are sensitive to sensors location [8]. Applying these methods in a specific order allow to overcome aforementioned drawbacks [9], but requires a huge amount of data in order to accurately determine damage location [10]. Moreover, if the structure is not equipped with a continuous monitoring system, using such a methodology needs to make post earthquake measurements that can be dangerous to perform. To deal with this issue, a relevant solution consists in coupling numerical modelling by Finite Element (FE) and OMA. Indeed, FE models can be used to quickly identify eigen frequency and modal shapes [11, 12], but also to simulate a damage state induced by an earthquake [13, 14].

After a short presentation of the chosen building (section 2), the numerical assumptions used to modelled the building and simulated its dynamic behaviour are described (section 3). The two computations methods (frequency and dynamic) are firstly introduced following by the material description and the

generation of artificial earthquake representative of the POCTEFA area. Results obtained are finally discussed and guidelines are given in view of the future instrumentation of the building (section 4).

2 Building description

The studied building is located in Andorre-la-Vieille (Edifici administratiu del Prat del Rull del govern d'Andorra, Fig 1-a). The structure built in 2013 is mainly constituted of reinforced concrete and exhibits two underground floors and six upper floors leading to a total height of $20.5\,\mathrm{m}$. The basement (approximately $37\,\mathrm{m}$ in width and $41\,\mathrm{m}$ in length, Fig 1-b) is supported by a 1-metre thick concrete screed and the two underground floors are sustained by concrete walls, beams and columns. Regarding the upper floors, slabs are composed of load-bearing Haircol® material and are sustained by metal beams. The link between the first level (over the ground) and the top of the building is mainly done by metal columns. Finally, a lift surrounded by concrete walls and two metal stairways allow to move within the building.

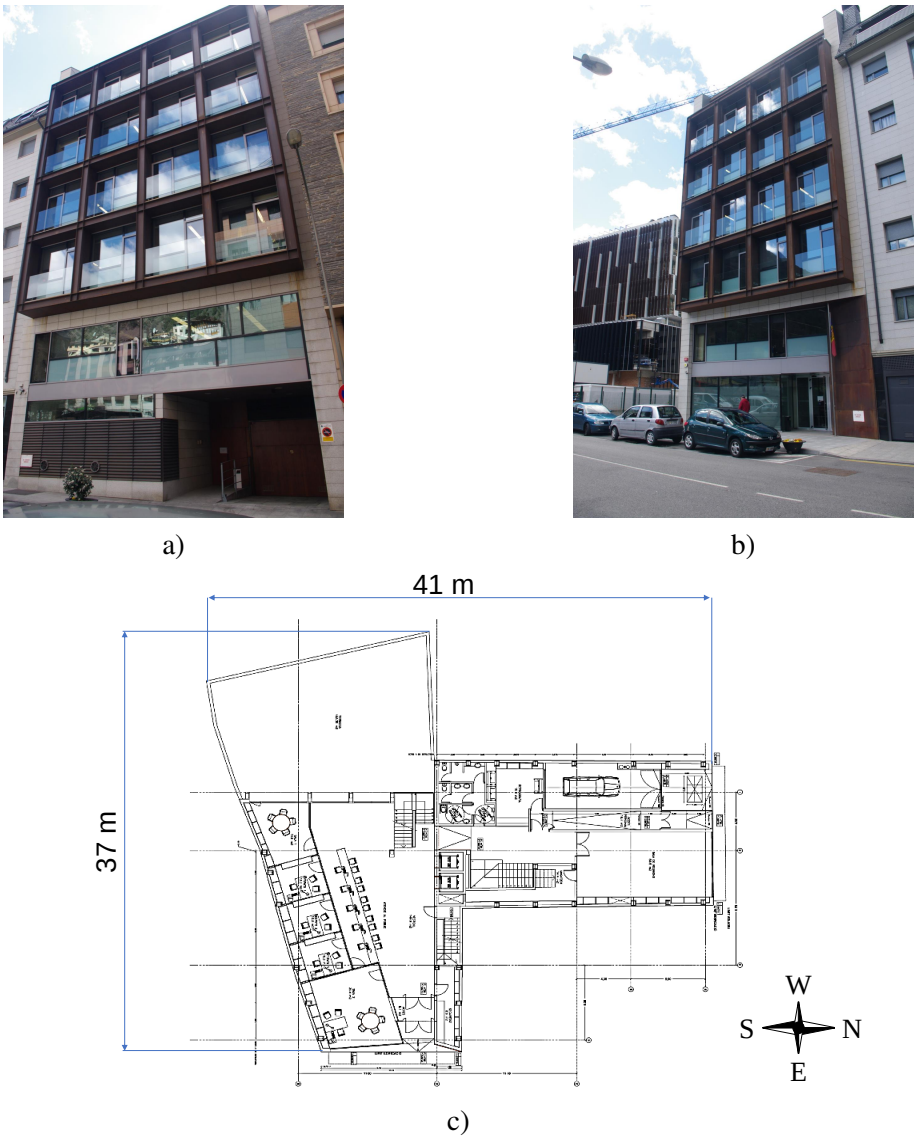

a) b) c)

FIGURE 1 – Edifici administratiu del Prat del Rull : (a) north facade, (b) east facade and (c) basement map

3 Numerical model

3.1 Computation methods

Two kind of computation methods implemented in the finite-element software Abaqus® are used in the following sections : a frequency computation method and a dynamic computation method. The first method corresponds to a linear perturbation procedure and allows the extraction of eigen frequencies and modal shapes of the structure at a given state [9]. Based on Lanczos algorithm, such approach includes initial stress and load stiffness effects due to preloads. It is thus necessary to use a static non-linear computation method in order integrate the proper weight of the structure before running a frequency computation study. The dynamic method provides a non-linear analysis of the structure and aims to simulate seismic events and induced damage [13, 14]. Since such procedure uses an explicit solver, the duration of the computation step is linked to the size of the smaller mesh element. Special attention must therefore be paid to mesh elaboration so as to minimize computation time.

3.2 Building modelling and numerical assumptions

Concrete elements (screed, slabs, walls, metal stairways, beams, columns) are modelled by shell elements while wire elements are used for metal elements (beams, columns and window frames). These modelling choices are motivated by the geometry of the structural elements (that exhibit higher width and length than their respective thickness) and in view of saving computation time. Indeed, due to the large dimension of the building, using 3D solid elements for all parts would involve a very long computation time. Respective thickness and cross section of shell and beam elements are then taken into account by defining section properties.

The complex and non-linear behaviour of concrete is simulated via Concrete Damage Plasticity (CDP) law and material density ($\rho = 2400\,\mathrm{kg}\cdot\mathrm{m}^{-3}$). This elasto-plastic damage model initially implemented within Abaqus® allows the recognition of crack patterns [15]. This model is governed by the following equation :

$$\sigma = (1-d)\, D_0^{el} : \left(\varepsilon - \varepsilon^{pl}\right) \tag{1}$$

where σ is the Cauchy stress tensor, d the scalar stiffness damage variable, ε the strain tensor, ε^{pl} the plastic strain tensor and D_0^{el} the undamaged elastic stiffness of the material. On the other hand, S355 steel exhibits an elastic behaviour with mechanical properties provided by architectural data (Young modulus : $E = 200\,000\,\mathrm{MPa}$, Poisson ratio : $\nu = 0.29$ and density : $\rho = 7800\,\mathrm{kg}\cdot\mathrm{m}^{-3}$).

Haircol® slab is composed of a concrete layer showing different thicknesses which is sustained by a metallic plate (Fig. 2). In view of further FE calculations, we intend to represent such complex structure by means of a simplified equivalent material, defined by its thickness and weight. To achieve this, an homogenization approach has been implemented upon the analysis of an elementary structure composed of two floors sustained by wire elements (simulating metal columns) embedded to the ground at their bases. Each floor is composed of four slabs linked together by tie interactions. Homogenized properties were then identified consequently to fit the eigen frequencies of the 3D Haircol® model. Modal shapes obtained for 3D and homogenized models (for a thickness of $0.092\,\mathrm{m}$ and a density of $\rho = 2018\,\mathrm{kg}\cdot\mathrm{m}^{-3}$) are compared on Fig. 3. Moreover, Table 1 gives the modal eigen frequencies in both cases for the two first flexion modes and for the first torsion mode. Deformation shapes match well

and a maximum relative difference of 6.66 % is obtained for the first flexion mode, which is clearly acceptable. Homogenizing Haircol® slab seems thus a relevant choice to provide a more easy-handling representation of the building.

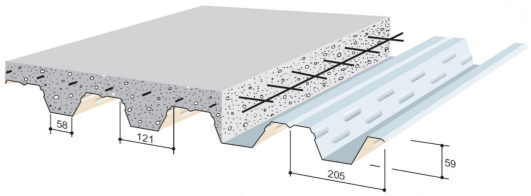

FIGURE 2 – Schematic representation of a Haircol® slab [16]

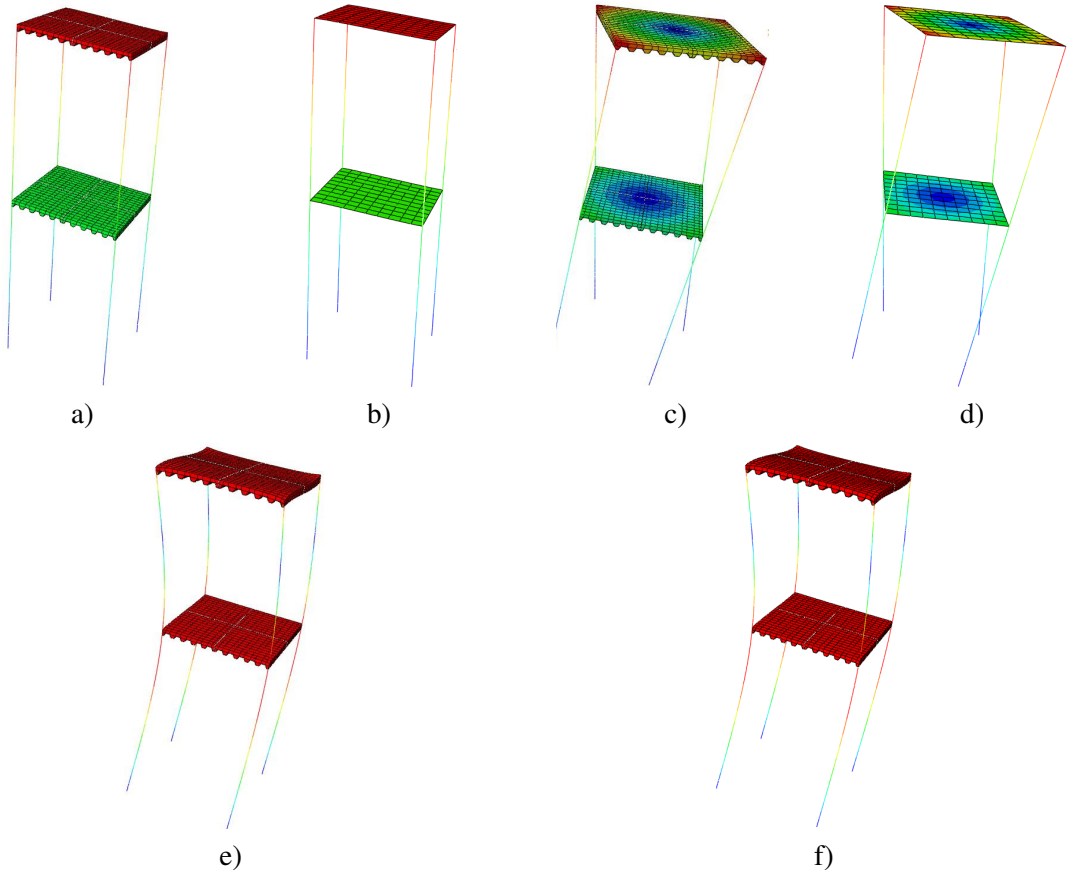

FIGURE 3 – Numerical results of the homogenization procedure : (a)/(b) : first flexion mode, (c)/(d) : first torsion mode, (e)/(f) : second flexion mode with (a), (c) and (e) corresponding to 3D model and (b), (d) and (f) to homogenized model.

	First flexion mode	**First torsion mode**	**Second flexion mode**
3D model	0.90 Hz	1.15 Hz	15.95 Hz
Homogenized model	0.96 Hz	1.21 Hz	15.93 Hz
Relative difference	6.66 %	5.21 %	−0.12 %

TABLE 1 – Comparison between the eigen frequencies of the 3D and homogenized models

Once each element is modelled, all shell elements are merged together to form one unique part in order to minimize the use of tie constraints. Tie constraints are finally applied between shells and wire elements to structurally link them together. The final geometry of the numerical model is presented on Fig. 4.

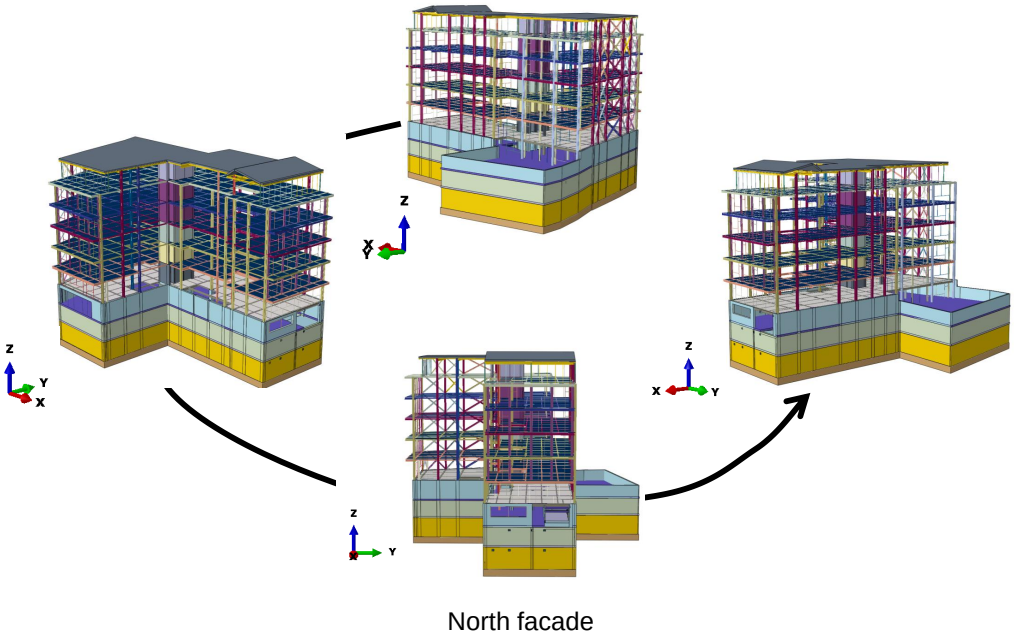

FIGURE 4 – Numerical model of the Edifici administratiu del Prat del Rull

Gravity and non-structural mass are then defined in order to integrate the proper weight of the structure and the initial stress of the structure. Gravity is applied on the whole model while non-structural is applied on each upper floor ($45\,\mathrm{kg}\cdot\mathrm{m}^{-2}$: representing an approximation of the weight office supplies) and the first underground floor ($125\,\mathrm{kg}\cdot\mathrm{m}^{-2}$: representing an approximation of the weight of parked vehicles and operational weight).

Regarding boundary conditions, conventional seismic analysis generally do not take into account the flexibility of the foundation and adjacent soil [11]. As a consequence, the evaluated seismic performance may be significantly different from that of the actual building [17]. In the present case, data on soil-structure interactions were not available. Yet, in view of the geological context (Pyrenees moutain, location altitude : $1023\,\mathrm{m}$), soil type can be considered as generic rock. It has thus been assumed to embed the base (underground floors) for frequencies computation. In the case of dynamic analysis, the embedding of the base is replaced by base motion accelerations along directions X, Y and Z. Precisely, the software Seismo Artif 2016 was used to generate synthetic accelerograms representative of seismic activity in the Poctefa region (French-Spanish-Andorran border). Pyrenees mountains are located within an interplate regions [18], and the maximum recorded magnitude was 6.5 [19]. In this study, the duration of the earthquake was arbitrary set to $5\,\mathrm{s}$. Fig. 5 shows the three accelerograms generated by Seismo Artif 2016.

The structure is finally meshed using 3D linear beams (B31), linear triangular and quadrilateral shells, respectively (S3R) and (S4R) elements (Fig. 6). A particular care is taken on mesh. Indeed, for dynamic computation methods, the duration of computation steps is closely linked to the size of the smaller element (L) and the speed of wave propagation (C_0) within material ($\delta t = \frac{L}{C_0}$). A convergence study has thus been conducted to ensure the results stability according to the mesh size leading to an average ele-

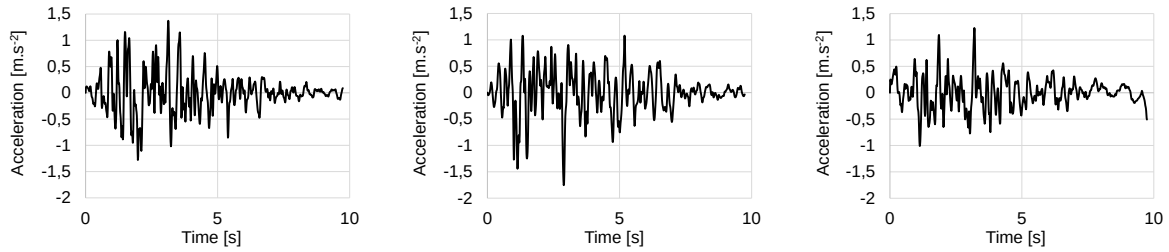

FIGURE 5 – Accelerations used to simulate the earthquake : (a) X direction, (b) Y direction and (c) Z direction

ment size of $0.5\,\mathrm{m}$. Precisely, the average aspect ratio ($\overline{\delta}$) is below 5 for the whole model which allows to minimize mesh distortion issues during the computation process. Details of the meshing characteristics (number and type of used elements and distortion criteria) are presented in Table 2.

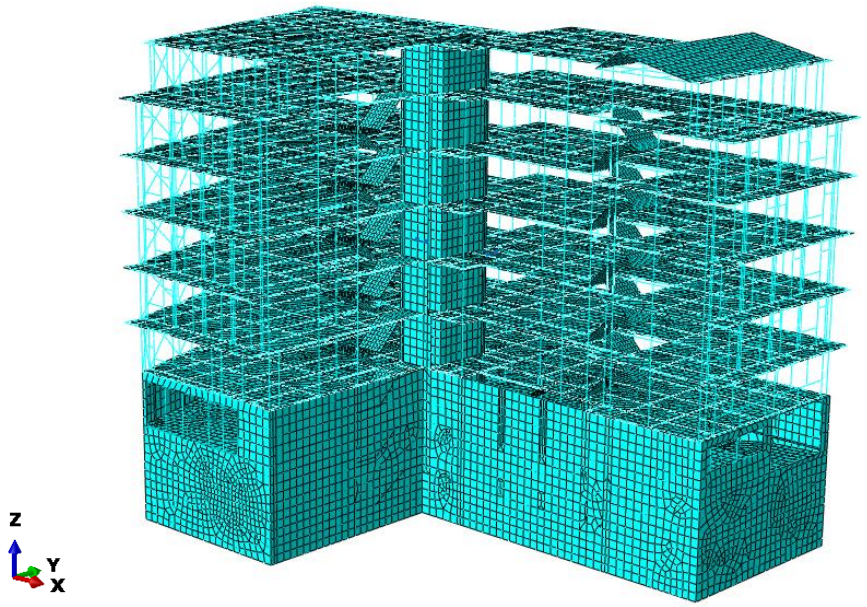

FIGURE 6 – Meshed structure

Element type	Number of elements	Average aspect ratio $\overline{\delta}$	Element with $\delta > 10$
Beam (B31)	9702	—	—
Triangular (S3R)	5271	4.26	$1.54\,\%$
Quadrilateral (S4R)	44821	1.40	$0.01\,\%$

TABLE 2 – Mesh characteristics

4 Results

4.1 Dynamic characteristics of the undamaged structure

Frequency computation is applied to the FE model presented bellow in order to study eigen frequencies and their associated modal shapes. The first 200 modal shapes have been evaluated in the aim to ensure that the Cumulative Effective Mass Participation Factor (CEMPF) corresponds to at least $80\,\%$ of the total mass of the building [11, 20]. The most important Effective Mass Participation Factors (EMPF) are obtained with the first modes of the structure (mode n^o 1, n^o 2 and n^o 4) for which the EMPF are higher than $7\,\%$ (Fig. 7 and Table 3). EMPF factors decrease then drastically with higher modes and numerous local and mixed modal shapes appear. Though the first modes induce a large movement of the upper part of the structure, the CMEPF reaches only a maximum of $23\,\%$ of the total mass of the building upon X direction (Fig. 8-a) and $22\,\%$ upon Y direction (Fig. 8-b). This result differs from classic results from literature [11], but can be explained by the singular constitution of the building. Indeed, the upper part of the building is mainly carried by metal beams and columns while the bottom part is entirely constituted of concrete. Moreover, the basement representing $66\,\%$ of the total weight is embedded within the soil. It results thus two distinct mechanical behaviours characterized by a higher flexibility of the upper part than those of the bottom part. Consequently, the upper part is subject to large displacements while the almost totality of the bottom part (underground floors) does not move. If the embedding of the underground storey is taken into account in calculating the CEMPF, this one reaches $80\,\%$ of the total mass from the mode n^o 4. It is thus relevant to consider that the dynamical behaviour of the structure is well described by the numerical model.

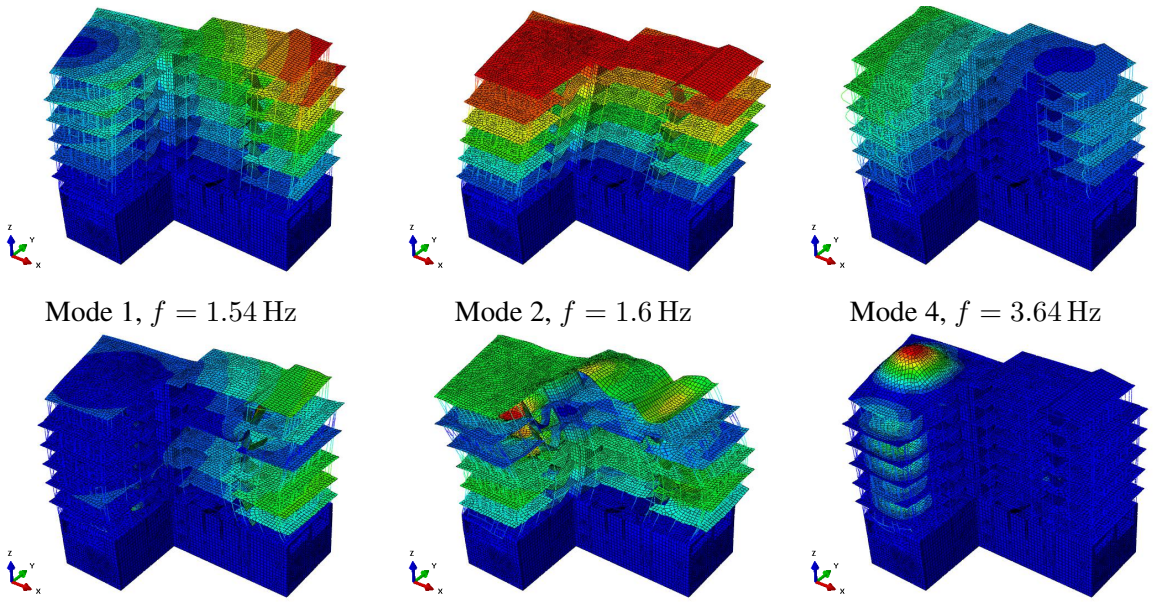

Mode 1, $f = 1.54\,\mathrm{Hz}$ Mode 2, $f = 1.6\,\mathrm{Hz}$ Mode 4, $f = 3.64\,\mathrm{Hz}$

Mode 75, $f = 4.93\,\mathrm{Hz}$ Mode 86, $f = 6.32\,\mathrm{Hz}$ Mode 171, $f = 8.12\,\mathrm{Hz}$

FIGURE 7 – Preponderant modal shapes

	Frequency	X EMPF	Y EMPF	Z EMPF
Mode n° 1	1.54 Hz	1.75 %	9.37 %	0 %
Mode n° 2	1.60 Hz	16.2 %	2.52 %	0 %
Mode n° 3	3.41 Hz	0 %	0 %	0.01 %
Mode n° 4	3.64 Hz	0.64 %	7.29 %	0 %
Mode n° 75	4.93 Hz	0.27 %	1.71 %	0.03 %
Mode n° 81	5.68 Hz	0.00 %	0.01 %	2.63 %
Mode n° 86	6.32 Hz	3.02 %	0.32 %	0.15 %
Mode n° 182	9.16 Hz	0.00 %	0.00 %	2.84 %

TABLE 3 – Sum of effective contributions upon directions X, Y and Z for the most heavy modes

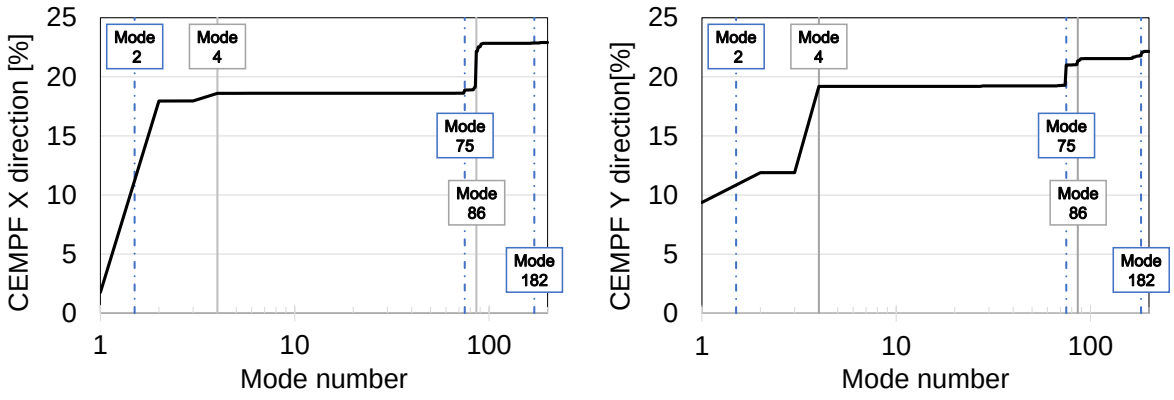

a) b)

FIGURE 8 – Modal analysis results : (a) CEMPF upon X direction (b) CEMPF upon Y direction

4.2 Damage process

The introduction of damage within the structure is achieved by the simulation of a magnitude 6 earthquake using a non-linear analysis. During a short period of time (approximately $0.5\,\mathrm{s}$) corresponding to the establishment of the seismic amplitude (Fig. 9), the kynetic energy of whole model increases slightly and stresses are mainly concentrated on metal beams around windows. At this time, a very weak strain energy is detected within the model as all structural elements remain in the elastic domain (as exemple : $\overline{\sigma}_{metal\ beams} \approx 26\,\mathrm{MPa} < \sigma_{pl} \approx 450\,\mathrm{MPa}$) and no damage is detected within the model (Fig. 10 and Fig. 11). Beyond this point, the kinetic energy continues to increase and strain energy begins to grow more significantly. A leap of kinetic energy appears then at $0.6\,\mathrm{s}$ leading to a sudden increase of strain energy. As a consequence, the plastic strain limit of concrete is reached in areas near windows and the building starts to be damaged. The seismic acceleration reached then an amplitude of $1.5\,\mathrm{m}\cdot\mathrm{s}^{-2}$ (in absolute value) along Y (corresponding East-West direction) leading to the increase of stresses and the exceeding of the elastic stress limit of metal beams located in this direction. It thus results a local increase in the forces transmitted from the metal structure to the concrete structure in these zones inducing thus the extension of the damaged zones and an increase of the loss of concrete stiffness linked with crack propagation. From this point, the computation process is stopped due to the apparition of large stresses within metal beams that create element distortion issues and because some areas along East-West direction exhibit $98\,\%$ of damage.

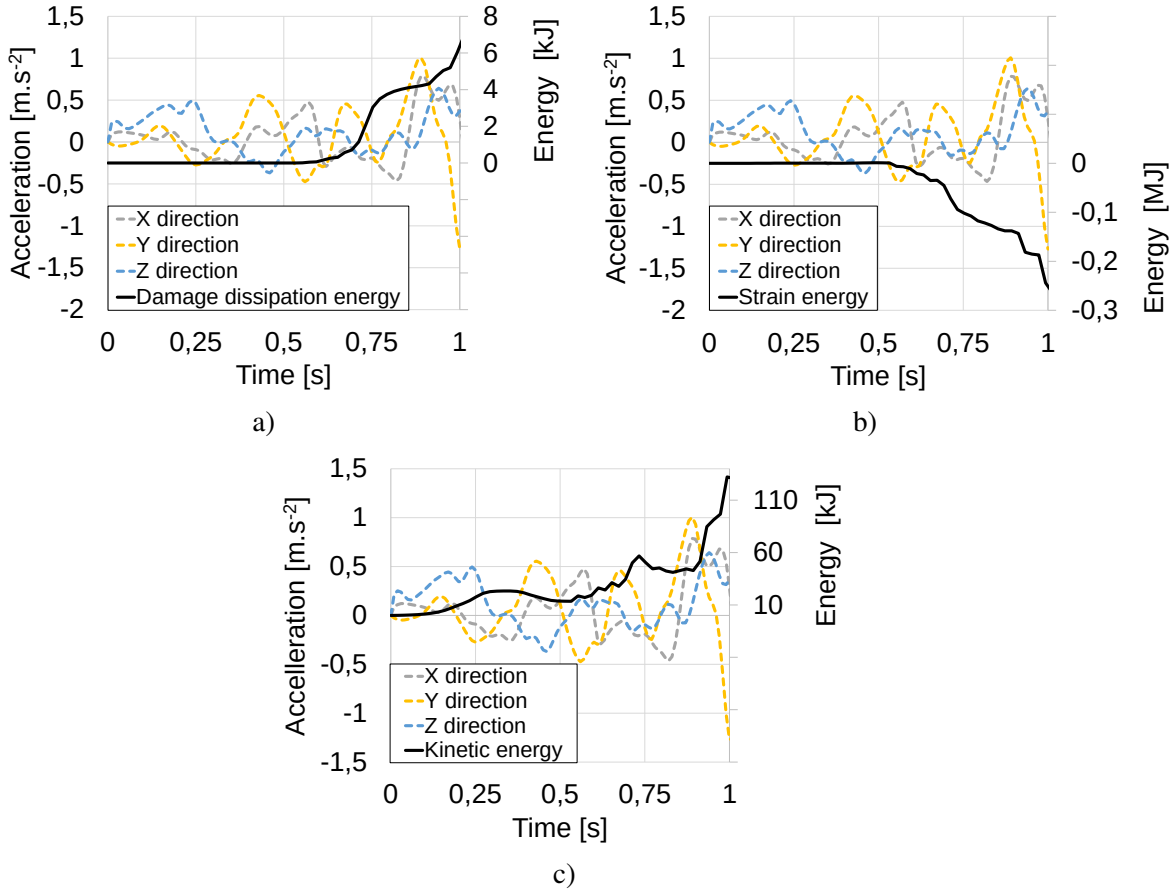

FIGURE 9 – Accelerations data along X, Y, and Z directions and evolution of energies within the model in function of time : (a) damage energy dissipation, (b) strain energy and (c) kinetic energy

4.3 Optimization of sensors positioning

Thanks to the results obtained through computational analysis, it is possible to optimize the location of sensors. On the one hand, the preponderant modal shapes extracted from the frequency analysis show a large sensibility of the building in regards with torsion and flexion modes, but also a weak motion of the underground floors due to the embedding with the ground of this part of the structure (Fig. 7). On the other hand, results obtained from the dynamical analysis show that stresses and strains are concentrated near the zones where windows are located. Setting-up multi-directional sensors (accelerometers) near windows that is to say near the corners of the building seems thus a relevant solution to capture both torsion and flexion modal shapes, but also accelerations induced by an earthquake. Using sensors in the underground levels of the building is however not necessary because of this weak motion. Indeed, accelerations would be hard to detect in these zones. Recommendations for sensors positioning are presented on the Fig. 12.

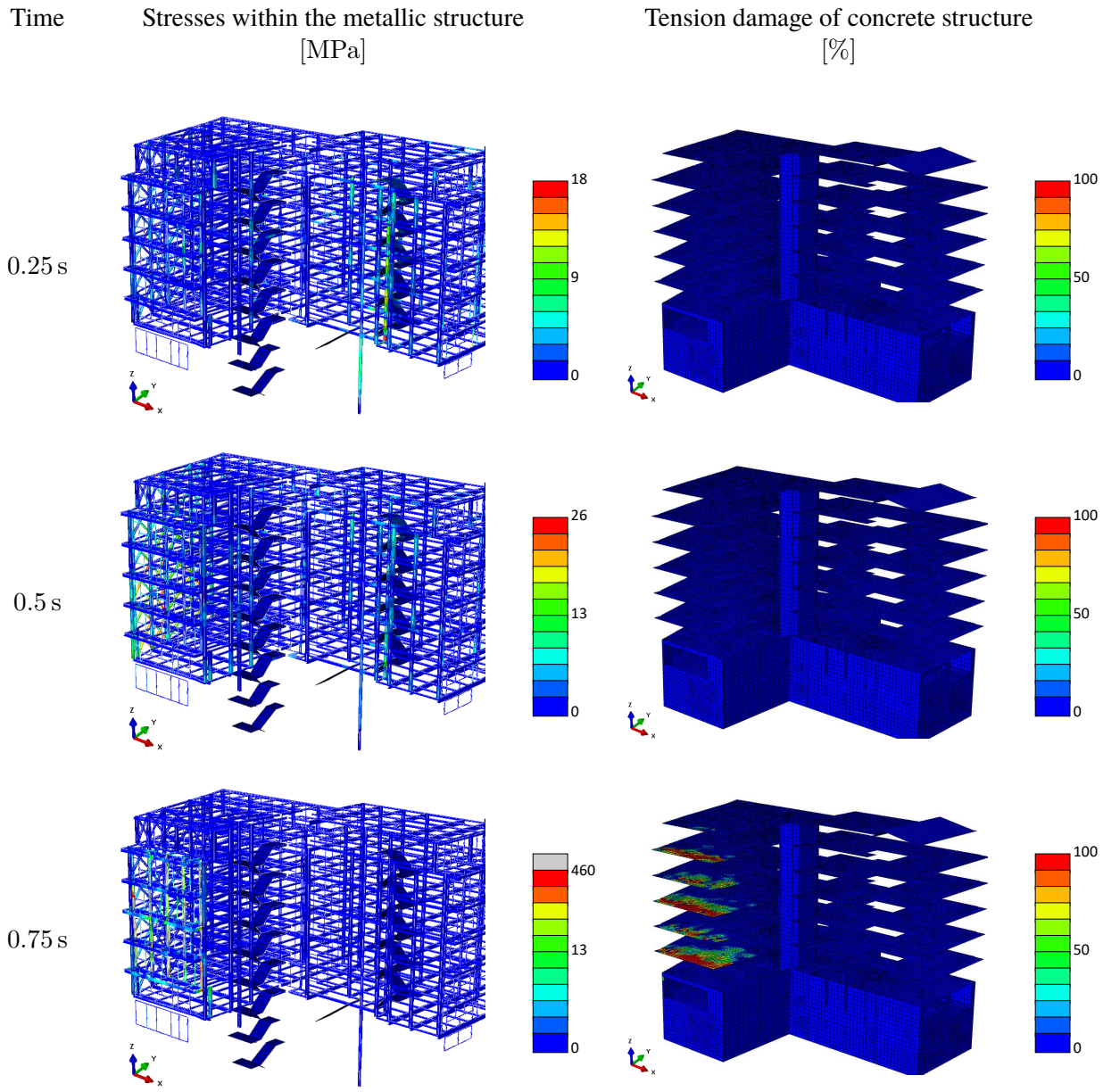

FIGURE 10 – Simulation of damage process following the North East direction

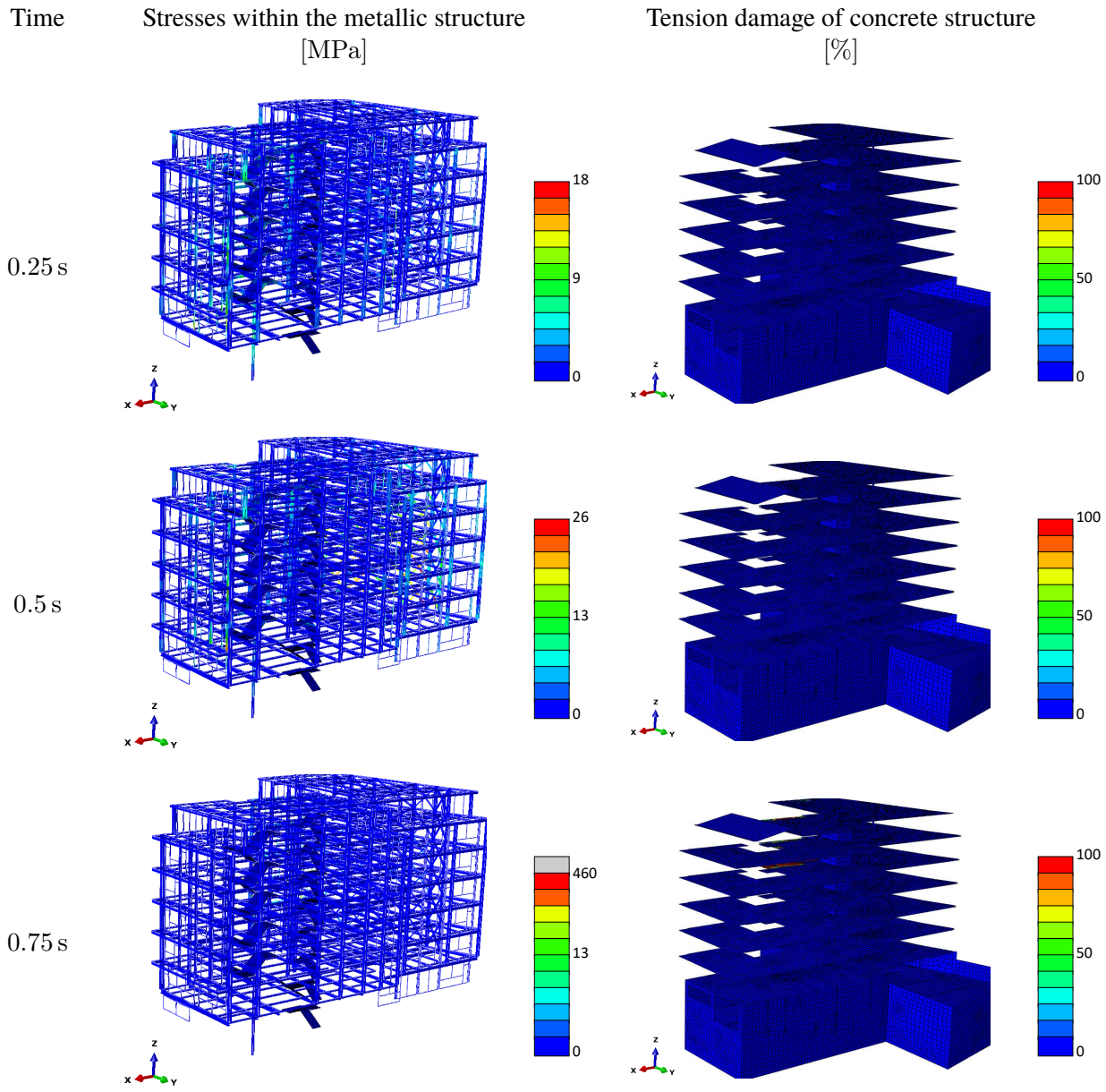

FIGURE 11 – Simulation of damage process following the North West direction

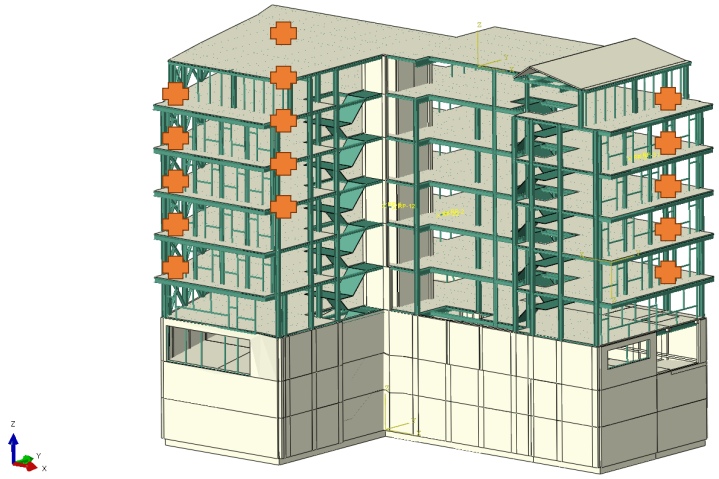

FIGURE 12 – Suggested location of sensors (represented by orange crosses)

5 Conclusions and perspectives

This paper assesses the seismic vulnerability of the Edifici administratiu del Prat del Rull del govern d'Andorra. To this purpose, the dynamic mechanical behaviour of the structure was studied through a finite element model. Dynamic characteristics of the undamaged structure (eigen frequencies and modal shapes) were firstly identified by linear perturbation procedure. A non-linear computation procedure was then used to simulate an earthquake representative of the local seismic activity to induce some damage. Using these results, optimization of the location of sensors (accelerometers) may be done within the structure to achieve its continuous monitoring. To go further, the numerical model could be calibrated using experimental data acquired by mean of accelerometers and real aperture radar. Indeed, such approach seems necessary to calibrate the soil/structure interactions and better represent the dynamic behaviour of the building.

Références

[1] A. Martin and M. Sevilla and J. Zurutuza Western Pyrenees geodetic deformation study using the Guipuzcoa GNSS network. *J. Appli. Geodesy*, Vol **12**, 229–238, 2018.

[2] http ://www.franceseisme.fr, 2019.

[3] S.K.U. Rehman and Z. Ibrahim and S.A. Memon and M. Jameel. Non destructive test methods for concrete bridges : A review. *Contr. Build. Mater*, Vol. **107**, 58–86, 2016.

[4] J.M. Ndambi andJ. Vantomme and K. Harri. Damage assessment in reinforced concrete beams using eigenfrequencies and mode shape derivatives. *Eng Struct*, Vol. **24**, 501–515, 2002.

[5] P. Guéguen and A. Tiganescu. Condition-based decision using traffic-light concept applied to civil engineering buildings. *Procedia Eng.*, Vol **199**, 2096–2101, 2017.

[6] A.K. Pandey and M. Biswas and M.M. Samman. Damage detection from changes in curvature mode shapes. *J. Sound. Vib.* Vol. **145**, 321–322, 1991.

[7] N. Cavalagli and G. Commanducci and F. Ubertini. Earthquake-induced damage detection in a monumental masonry bell-tower using long-term dynamic data monitoring. *J. Earthq. Eng.*, Vol. **22**, 96–119, 2018.

[8] F. Frigui Contribution au développement d'un système de surveillance en génie civil. *PhD Thesis*, Institut National Polytechnique de Toulouse, 2018.

[9] F. Frigui and J.P. Faye and C. Martin and O. Dalverny and F. Peres and S. Judenherc Global methodology for damage detection and localization in civil engineer structures. *Eng. Struct.*, Vol. **171**, 686–695, 2018.

[10] V.B. Dawari and G.R. Vesmawala. Structural damage identification using modal curvature differences. *J. Mech. Eng.*, Vol. **4**, 33–38, 2013.

[11] F. Clementi and V. Gazzani and M. Poiani and S. Lenci Assessment of seismic behaviour of heritage masonry buildings using numerical modelling. *J. Build. Eng.*, Vol. **8**, 29–47, 2016

[12] A. Cabboi and C. Gentile and A. Saisi. From continuous vibration monitoring to FEM-based damage assessment : Application on a stone-masonry tower. *Contr. Build. Mater*, Vol. **156**, 252–265, 2017.

[13] E. Ercan and B. Arisoy and E. Hökelekli and A. Nuhoğlu. Estimation of seismic damage propagation in a historical masonry minaret. *J. Eng. Nat. Sci.*, Vol. **35**, 647–666, 2017.

[14] I. Roselli and M. Malena and M. Mongelli and N. Cavalagli and M. Gioffrè and G ; De Canio and G. De Felice. Health assessment and ambient vibration testing of the « Ponte delle Torri » of Spotelo during the 2016-2017 Central Italy seismic sequence. *J. Civ. Struct. Health Monit.*, Vol. **8**, 199–216, 2018.

[15] T. Jankowiak and T. Lodygowski. Identification of parameters of concrete damage plasticity constitutive model. *Found Civ Environ Eng*, Vol. **6**, 53–69, 2005.

[16] http ://ds.arcelormittal.com, 2019.

[17] M Li and X Lu and X Lu and L Ye. Influence of soil-structure interaction on seismic collapse resistance of super-tall buildings. *J. Rock Mech. Geotech. En*, Vol. **6**, 477–85, 2014.

[18] P.G. Fitzgerald and J.A. Munoz and P.J. Coney and S.L. Baldwin. Asymmetric exhumation across the Pyrenean orogen : implications for the tectonic evolution of a collisional orogen. *Earth Planet. Sc. Lett.*, Vol. **173**, 157–170, 1999.

[19] J. Garcia and J.M. Insua-Arévalo. Seismic hazard for the Itoiz dam site (Western Pyrenees, Spain). *Soil Dyn. Earthq. Eng.*, Vol. **31**, 1051–1063, 2011.

[20] M.S. Ahmad and M. Jamil and J. Iqbal and M.N. Khan and M.H. Malik and S.I. Butt Modal analysis of ship's mast structure using effective mass participation factor. *Indian J. Sci Technol.*, Vol. **9**, 21, 2016